frontiers in Materials

ORIGINAL RESEARCH
published: 07 January 2022
doi: 10.3389/fmats.2021.812402

Mechanical Characteristics and Stress Evolution of Cemented Paste Backfill: Effect of Curing Time, Solid Content, and Binder Content

Chen Hou[1]*, *Liujun Yang*[1], *Lei Li*[1] and *Baoxu Yan*[2]

[1]Center for Rock Instability and Seismicity Research, School of Resource and Civil Engineering, Northeastern University, Shenyang, China, [2]Energy School, Xi'an University of Science and Technology, Xi'an, China

The clarification of the variation on the strength of the cemented paste backfill (CPB) under the coupling of multi-factor is the foundation of the CPB design of the mine. In this article, the physical and mechanical properties of the CPB under the coupling effect of curing time, solid content, and binder content were experimentally and theoretically investigated. The results show that 1) the increase in binder content can effectively increase the later strength of CPB. 2) A sensitivity parameter considering the span of multi-factor was constructed, indicating that the curing time has the greatest impact on the uniaxial compressive strength (UCS), and the variation in solid content has the least impact on it, which can be verified by the stress–strain curves. 3) Curing time and binder content can effectively change the stress evolution, which is reflected in reducing the strain corresponding to the peak stress, enhancing the characteristics of the peak stress and increasing stress drop. The results of this study aim to explain the essence of the influence of each factor on the mechanical behavior of CPB in the view of stress–strain evolution, which will help to better understand the mechanical characteristics of CPB and quantify the sensitivity of the mechanical properties to various factors.

Keywords: cemented paste backfill, multi-factor, uniaxial compressive strength, sensitivity analysis, stress–strain behavior

OPEN ACCESS

Edited by:
Lijie Guo,
Beijing General Research Institute of Mining and Metallurgy, China

Reviewed by:
Zhihong Zhang,
Beijing University of Technology, China
Ferdi Cihangir,
Karadeniz Technical University, Turkey

***Correspondence:**
Chen Hou
houchengood@yeah.net

Specialty section:
This article was submitted to Structural Materials, a section of the journal Frontiers in Materials

Received: *10 November 2021*
Accepted: *06 December 2021*
Published: *07 January 2022*

Citation:
Hou C, Yang L, Li L and Yan B (2022) Mechanical Characteristics and Stress Evolution of Cemented Paste Backfill: Effect of Curing Time, Solid Content, and Binder Content. Front. Mater. 8:812402. doi: 10.3389/fmats.2021.812402

INTRODUCTION

With the demands of social development and the rapid economic development, mining activities are becoming more and more active all over the world. As a byproduct in the mining process, tailings are accumulated as solid waste from mining when recovering valuable mineral resources. It is estimated that the global annual discharged tailings is between 5 and 7 billion tons (Edraki et al., 2014). However, China's annual discharged tailings exceed 1 billion tons, with the total emission amounting to 10 billion tons (Rong et al., 2017). These massively discharged tailings will inevitably pose a serious threat to the environmental protection and safe production of mines.

Therefore, the safe and effective disposal of tailings under severe background is a mining engineering problem that needs to be solved urgently. The mine backfill method, a safe, environmentally friendly, and efficient method, has been widely used in underground mines (Yilmaz, 2011; Gorakhki and Bareither, 2017). Generally, the cemented paste backfill (CPB) is an engineered mixture of tailings, water, and hydraulic binders (2–9% by weight). It contains typically between 65 and 85% solids (Ercikdi et al., 2014; Cao et al., 2021). In mine production, goaf

management, mine environmental protection, and mine economic benefits, it has multiple advantages such as supporting goafs, increasing ore recovery rate, controlling surface subsidence, reducing tailings accumulation, and reducing tailings recovery costs (Wu et al., 2015; Sun et al., 2018). Therefore, it is widely used in mining and management of mines all over the world (Ding et al., 2018; Jiang et al., 2018; Mu et al., 2019). However, the prerequisite for the successful application of filling mining method in mines is the reasonable setting of CPB strength (Deng et al., 2017; Cao et al., 2018).

The uniaxial compressive strength is considered to be one of the important parameters in the design of underground mine operations, so scholars have carried out research on it. Deng et al. (2021) carried out the uniaxial compressive strength test and porosity determination test, which showed that the total porosity decreased and the CPB strength increased with the curing time. Li et al. (2020) designed the uniaxial compression test that considers the solid content of 65, 67, and 69% and cement–tailing ratio of 1:4, 1:10, and 1:20, and the result showed that the UCS increases with the increase in solid content and cement–tailing ratio. Ghirian and Fall (2016) showed that the curing stress can significantly affect the strength of CPB, for which the UCS of CPB was increased with the curing stress within a certain range. Hou et al. (2020) investigated the influence of curing time on the damage characteristics and energy dissipation of CPB. The results show that the prolongation of curing time can effectively hinder the initiation and expansion of cracks in the specimen to improve the UCS of the CPB. The strain energy and energy storage limit required for the deformation and failure of the CPB increase with the longer curing time. Hou et al. (2018) used fiber Bragg gratings to monitor the temperature and internal strain evolution of the after 7-day cured cemented tailings backfill (CTB) specimens. The results show that the binder content has a significant effect on the temperature and internal strain. CTB with a high binder content takes less time to reach the skeleton formation stage. Ghirian and Fall (2014) studied the evolution of coupled thermal, hydraulic, mechanical, and chemical properties of underground CPB by the insulated-undrained high column test. The results have demonstrated that the UCS values significantly increase with time due to the cement hydration process and suction development. Chen et al. (2021) showed that the increase in curing stress and curing temperature will increase cement hydration products to enhance UCS. Kesimal et al. (2005) showed that the binder mixtures can effectively increase the strength of CPB produced from sulphide rich tailings. Wu et al. (2020) indicated that increasing the curing humidity helps the hydration cycle, thereby generating more products to enhance the strength of CPB. Li et al. (2020) showed that a 2% increase in solid content (65, 67 and 69 wt%) results in a 55–88% increase in yield stress. Xu et al. (2018) constructed the relationship between UCS and electrical resistivity of CPB. UCS and electrical resistivity increased with increasing cement-to-tailing ratio, solid content, and curing time.

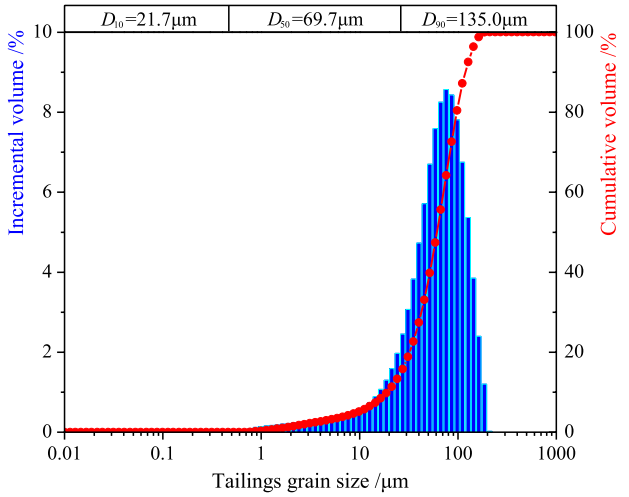

FIGURE 1 | Particle size distribution of tailings.

TABLE 1 | The main chemical composition of tailings.

Material	Composition						
Tailings	SiO_2	Al_2O_3	K_2O	TiO_2	Fe_2O_3	CaO	P_2O_5
	93.214	4.984	1.271	0.245	0.227	0.022	0.016

TABLE 2 | Main chemical composition of PCI-I.

Material	Chemical composition						
PCI-I (%)	CaO	SiO_2	Al_2O_3	Fe_2O_3	MgO	SO_3	K_2O
	43.648	33.930	12.381	3.265	2.655	1.674	1.516

To sum up, the scholars used indoor tests to analyze the effects of single or two factors on the strength of the CPB. However, the mine condition in different regions has obvious differences and particularities. Therefore, it is extremely important to consider the coupling of multiple internal factors in the process of designing backfill that meet the needs of different mines according to the mine situation. However, the current research status is relatively lacking. For this reason, combining the shortcomings of the above research fields, the investigation of the strength variation of the CPB were carried out under multi-factor coupling in the time domain, which can provide a reference for the design of the strength of CPB under different conditions.

This article is to consider multi-factors and adopt multiple methods to explore the evolution mechanism of the CPB in the strength. XRD technology was used to analyze the formation mechanism of the CPB strength by consideration of curing time, solid content, and binder content, and the uniaxial compression test was carried out to measure the UCS of CPB. The influence of multi-factor on strength was quantitatively analyzed by introducing sensitivity parameter *S*. Meanwhile, the

TABLE 3 | The growth rate of UCS with curing time.

Soild content (%)	x_1-x_2	3 (%)	5 (%)	7 (%)	9 (%)
Binder content (%)					
68	1d-3d	10.34	27.76	34.64	39.32
	3d-7d	0.59	6.40	10.61	3.68
	7d-14d	1.38	1.23	1.86	2.98
	14d-28d	0.83	0.98	0.96	0.86
72	1d-3d	11.05	22.13	33.60	32.32
	3d-7d	3.13	3.64	2.97	7.10
	7d-14d	0.05	2.15	2.08	1.86
	14d-28d	1.24	0.58	1.56	1.60
76	1d-3d	12.13	13.80	35.03	18.79
	3d-7d	2.77	3.22	2.31	5.73
	7d-14d	0.88	0.49	1.21	2.76
	14d-28d	0.42	0.60	1.34	0.80

Note: $r = \frac{(UCS_i - UCS_0)}{UCS_0 (x_1 - x_2)} r$ *is growth rate of UCS,* UCS_i *is the strength after the change,* UCS_0 *is the strength of the reference condition, and* x_1-x_2 *is shown in* ***Table 3***.

stress–strain curves were used to analyze the difference of the stress evolution under the influence of multi-factor, and the essence of the influence of multi-factor on the mechanical properties of the CPB was clarified.

EXPERIMENTAL PROGRAM

Materials

Tailings

This article selects synthetic silica tailings (ST) as the test aggregate to achieve the test purposes: 1) The simplicity of the mineral composition and chemical elements of ST can avoid the differential process of cement hydration so that the test results are reasonably explained. 2) Because of the long duration of the test, it can avoid the difference in chemical stability and mechanical properties of the CPB caused by the different pouring time. The particle size distribution with finer particle sizes of the tailing was selected according to the engineering application (Xincheng Gold in Shandong province, China) as shown in **Figure 1**. The main chemical compositions of tailings determined by x-ray fluorescence spectroscopy were listed in **Table 1**.

Hydraulic Binder

Portland cement Type I was used as the binder. The main chemical composition is shown in **Table 2**.

Mixing Water

Deionized water was used as the mixing water to prepare the slurry to ensure that the components in the mixing water would not affect the test results.

Testing Procedures

Specimen Preparation

Considering the solid content (68, 72, and 76%), binder content (3, 5, 7, and 9%), and curing time (1, 3, 7, 14, and 28 days) as influencing factors, the specimen preparation was carried out as follows: the required tailings, cement, and deionized water were calculated and weighed. After mixing the tailings and cement evenly, pour into deionized water and stir for 7 min. The slurry was poured into a cylindrical standard mold with a diameter of 50 mm and a height of 100 mm for uniaxial compression tests. Specimens were removed from molds after 24 h and were placed in a standard curing chamber at 20°C. In addition, the specimens were sealed before being placed in the chamber to prevent the influence of moisture in the curing chamber on the hydration reaction, and then the specimens were taken out to carry out the test when it reaches the specified curing time.

TABLE 4 | Sensitivity parameter values of factors.

Factor	Variable value (m_{ij})	$\Delta R/R_0$	Sensitivity parameter (S)
Curing time	3d	37.58%	0.188
	7d	84.92%	0.142
	14d	151.35%	0.116
	28d	205.49%	0.076
Solid content	72%	12.24%	0.009
	76%	31.28%	0.012
Binder content	5%	53.41%	0.059
	7%	176.10%	0.098
	9%	320.14%	0.119

Testing and Analysis Method

To obtain the physical and mechanical properties of specimens under different test conditions in the time domain, XRD component analysis test and uniaxial compression test were carried out.

XRD test was carried out by used Bruker D8 Advance x-ray powder diffractometer, which uses a copper target with a wavelength of 0.15418 nm. The composition analysis of the cement paste that had reached the designated curing time was carried out. The samples were crushed first, and the hydration reaction of the cement paste was terminated with ethanol, then dried, and sieved to prepare the samples for XRD component analysis. The continuous scanning time was 2°/min, and the scanning angle range was 5°–50°.

When the specified curing time was reached, the cylindrical specimen was taken out to be tested from the chamber. The uniaxial compression tests were carried out according to ASTM C39. Additionally, three specimens were tested at each condition. A mechanical loading system was used to conduct uniaxial tests to evaluate the mechanical properties of the CPB specimen, and the loading rate was 0.3 mm/min. The displacement and pressure were monitored by the laser displacement sensor and the pressure sensor during loading. The axial strain and stress of the specimen during the uniaxial compression process were calculated, and the stress–strains curves of different conditions were shown.

In order to explore the sensitivity of UCS to curing time, solid content, and binder content, the parameter N_i was introduced to normalize the range of factors. Then, the parameter S was introduced to calculate the sensitivity coefficient when factors change and to quantify the sensitivity of the UCS to each factor.

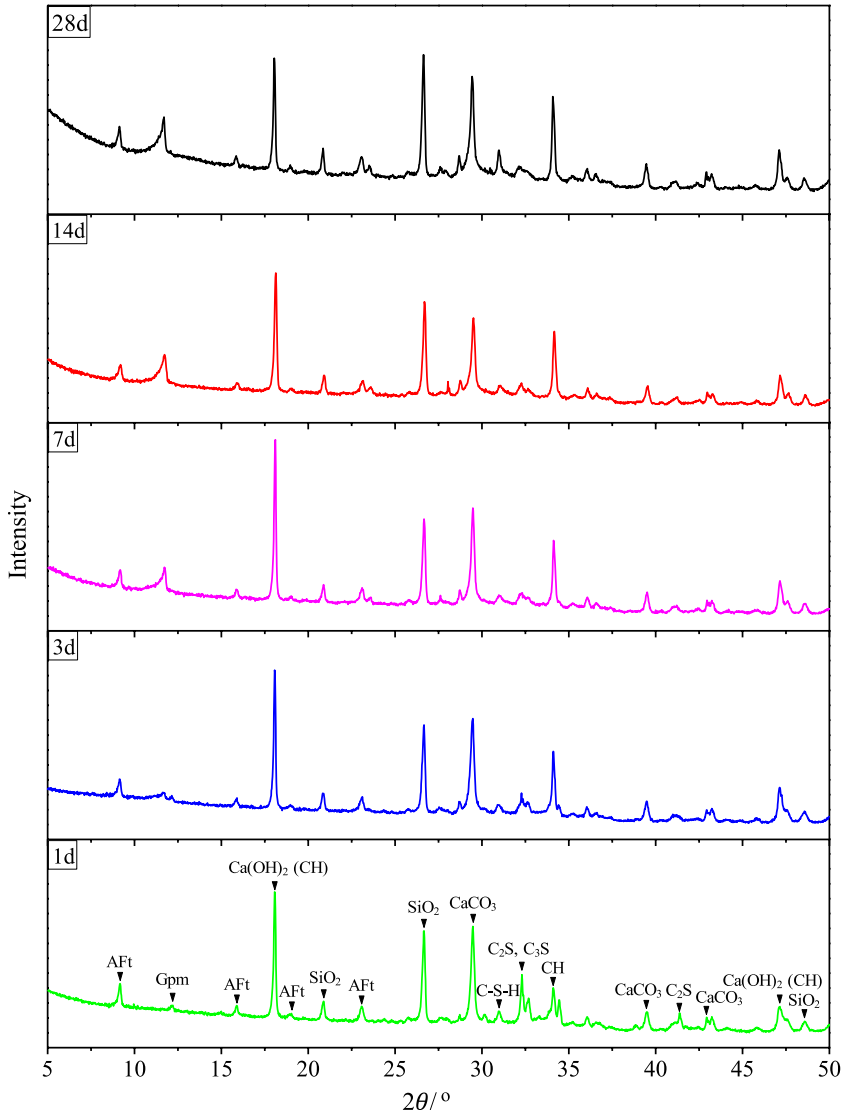

FIGURE 2 | XRD patterns of hydration products on CPB.

RESULTS AND DISCUSSION

Characteristics of Hydration Products on CPB

It can be seen from **Figure 2** that the hydration products changes with the curing time. In the early curing time, gypsum and cement clinker are disintegrated, dispersed, and suspended in the liquid under the action of higher moisture content and dissolved to produce SO_4^{2-}, Ca^{2+}, OH^-, and Al $(OH)^-$, which provide an ionic foundation for the production of Aft (Ettringite). In the early hydration, the hydration reaction of C_3A ($3CaOAl_2O_3$) is relatively active. Therefore, it is conducive to the production of AFt. With the continuous dissolution of the components in the cement, the increase in ion concentration, and the continuous progress of the hydration reaction, $Ca(OH)_2$ reaches a larger value when the curing time is 3 days after the unsaturated, saturated, and supersaturated stages. Then, its content declined as the curing time increased (Ma et al., 2019). The hydration reaction of C_3S generates C-S-H gel and CH after the first hydration reaction of C_3A. Therefore, the C_3S content decreases as the hydration reaction deepens, and the C-S-H gel content increases as the curing time increases (Cui and Fall 2016).

Variation of UCS Under the Multi-Factor Coupling

Variation of Curing Time on UCS

According to the curve between the curing time and UCS from **Figure 3**, it can be seen that UCS shows the same increasing trend with curing time, that is, it shows a parabolic shape, and the growth rate of UCS increases with curing time, as shown in **Table 3**. The

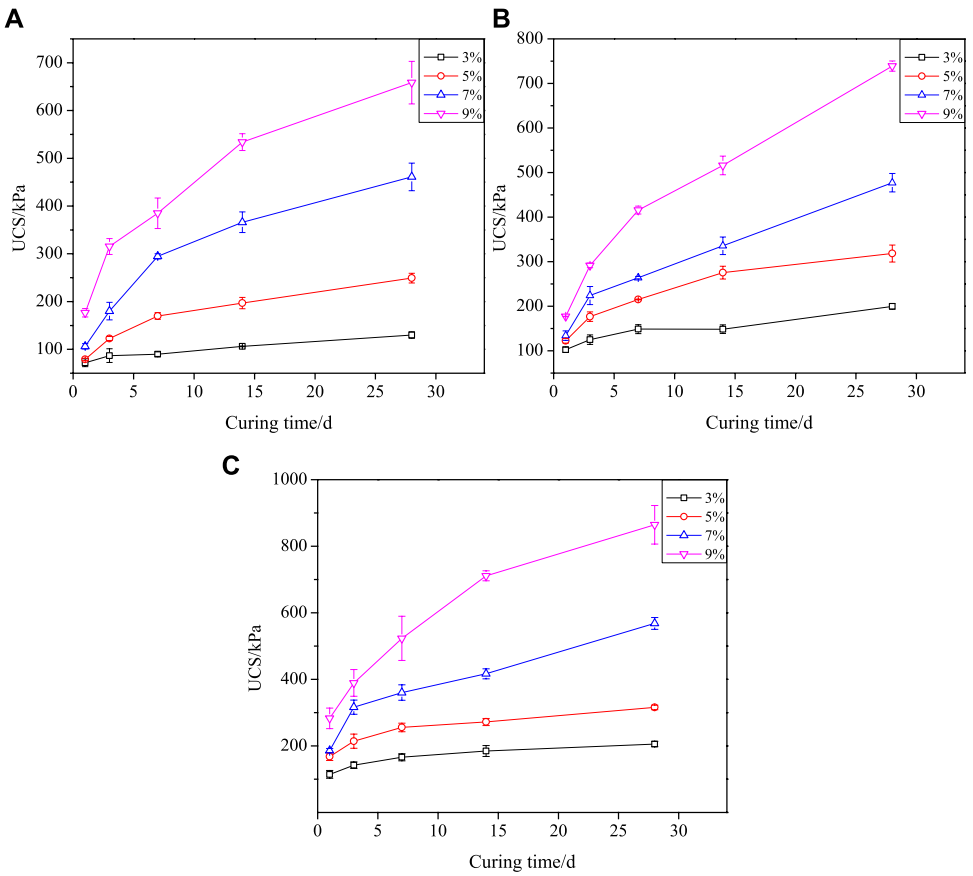

FIGURE 3 | The value of UCS corresponding to curing times under different solid content. **(A)** 68% solid content **(B)** 72% solid content **(C)** 76% solid content.

growth of UCS increases at the highest rate from 1 to 3 days, and the value can reach up to 39.32%, which corresponds to a 68% solid content and 9% binder content. After that, the growth rate of UCS decreases gradually when the curing time increases.

The essence of curing time reflects the degree and process of the hydration reaction. In the early hydration process of CPB, the space filling effect of AFt crystals is the main reason for the early strength of CPB (Xu et al., 2013). However, flocculent C-S-H gel, needle-shaped AFt crystals, and cement particles have not fully participated in the hydration reaction, and discrete tailings particles form a loose structure, which makes the early strength of CPB lower. With the increase in hydration degree, the AFt crystals are formed in large quantities and distributed in clusters, and contact points are formed with the increasing quantities of C-S-H gels (Zhang et al., 2018). The water-filled space is constantly being filled and the gap is reduced by hydration products, and the strength of CPB is continuously increasing; when the curing time at 28 days, the hydration process is gradually complete, a large amount of C-S-H gel is formed in CPB, and meanwhile, AFt crystals and $Ca(OH)_2$ crystals are completely formed. The hydration products are evenly distributed, interconnected, and intertwined (Hu et al., 2018). Hydration products, hydration particles, and tailings are complexly combined in the space to form a dense and stable multilayer network structure, which makes the CPB have long-term strength and sufficient resistance to external loads (Hu et al., 2018). The binder content increases as the solid content and binder content increase, and the cement particles that can participate in the hydration reaction increase. The hydration products generated by the hydration reaction develop into a denser and stable bearing structure, which strengthens the densification of the structure and has a stronger compressive strength.

Variation of Binder Content on UCS

The value of UCS increases with the increase in the binder content and the increase rate is significantly affected by the curing time from **Figure 4**. In the early period of the hydration reaction, the content of hydration products is low and a stable supporting framework structure has not yet formed. At the same time, sufficient water in the pores increases the lubrication between tailings particle, hydration products, and hydration raw materials. Therefore, when the curing time is 1 day, the increase in UCS caused by the increase in binder content is relatively small. With the increase in the curing time, higher initial binder content increases the amount of the hydration product, and the generated hydration products fill the water-filled space between the pores. The well-connected pore network gradually transforms into a dense supporting framework formed by the interlacing of hydration products, which made the CPB to

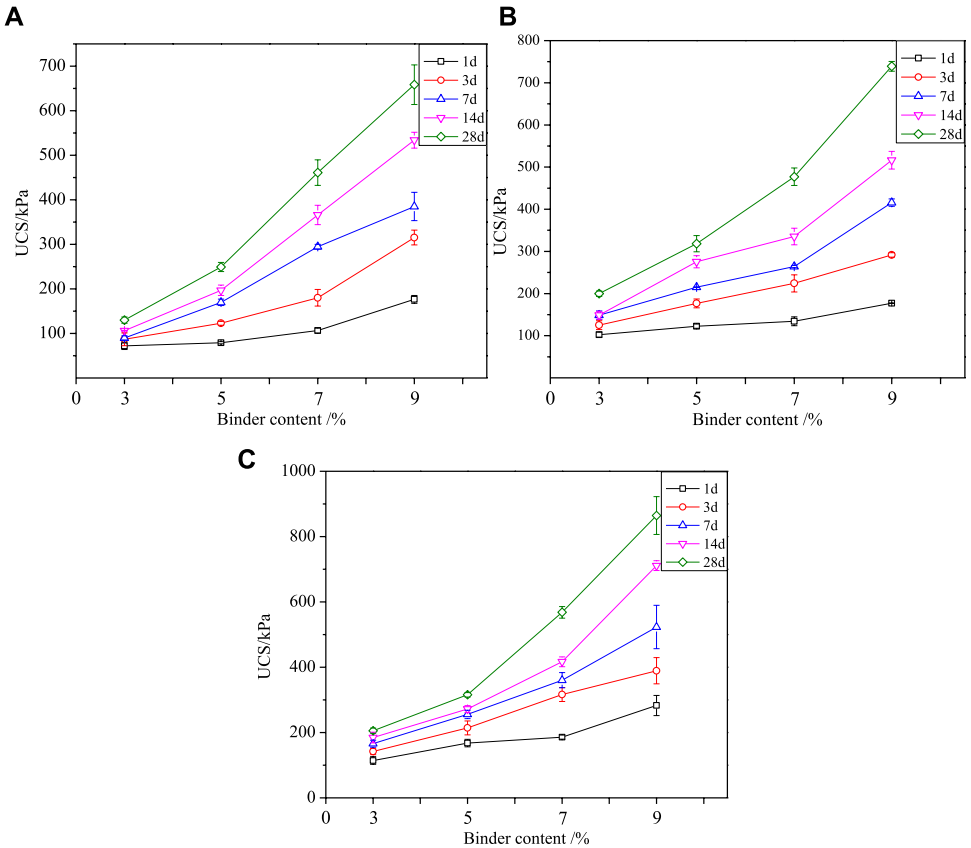

FIGURE 4 | The value of UCS corresponding to binder content under different solid content. **(A)** 68% solid content **(B)** 72% solid content **(C)** 76% solid content.

have higher strength with the increase in binder content. When the curing time is 28 days, it can be observed that UCS exhibits a relatively obvious increasing trend under the influence of binder content. That is, with the hydration reaction gradually becoming integrity, the influence of the binder content on UCS gradually appears, indicating that the increase in the binder content can effectively increase the advanced age of strength.

Variation of Solid Content on UCS

The UCS shows an increasing trend as the solid content from **Figure 5**. At the early curing time, the volume of air and free water in the pores of the CPB sample is relatively small as the solid content, which effectively reduces the connection and penetration of the pores, and forms an effective contact framework between tailings particles, hydration products, and unhydrated cement particles (Liu et al., 2020). The CPB with higher solid content has more particles (Liu et al., 2021). The load-bearing framework formed between the tailings particles and the unhydrated cement particles to form an effective lap between the solid particles. With the gradual advancement of the hydration process, the amount of hydration products produced in CPB with higher solids content increases and the degree of development is improved. The self-desiccation of CPB in the hydration process not only reduces the water-filled space in the pores but also provides development space for the generation and development of hydration products. The spatial distribution of hydration products greatly improves the framework structure of CPB, which fills the pore space and creates bonds between the particles (Ercikdi et al., 2014). The complex, dense, and stable load-bearing system is formed that combines a gel network composed of hydration products and a solid particle structure dominated by tailings. In other words, the enhancement of cohesion of structure effectively improves the later mechanical strength.

Sensitivity Analysis of Multi-Factor on UCS

It can be seen from the above results that the curing time, binder content, and solid content can all affect the value of UCS. In order to describe the effect of the three on the UCS, the three-dimensional coordinate system is constructed with the binder content (*X* axis), solid content (*Y* axis), and curing time (*Z* axis) as the coordinate axis and color to distinguish the value of the UCS under different conditions, as shown in **Figure 6**.

According to the value of UCS under different conditions, 68%, 72%, and 76% solid content are indicated by circles, squares, and triangles, respectively. It can be known from the color distribution of the spheres that the smaller values of UCS are mainly concentrated in the lower left area, and the color change difference is small along the *Y* axis, which means that the smaller UCS is determined by the shorter curing time and the lower binder content, and the increase in the solid content contributes relatively little to the increase in the UCS. The

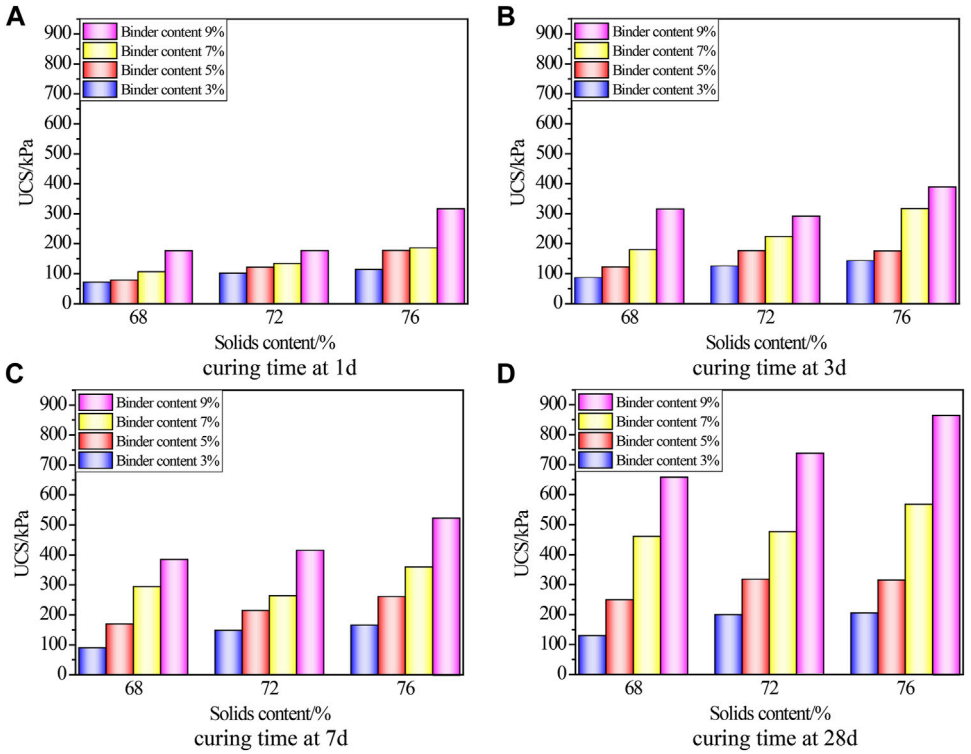

FIGURE 5 | The value of UCS corresponding to binder content under different cutting time.

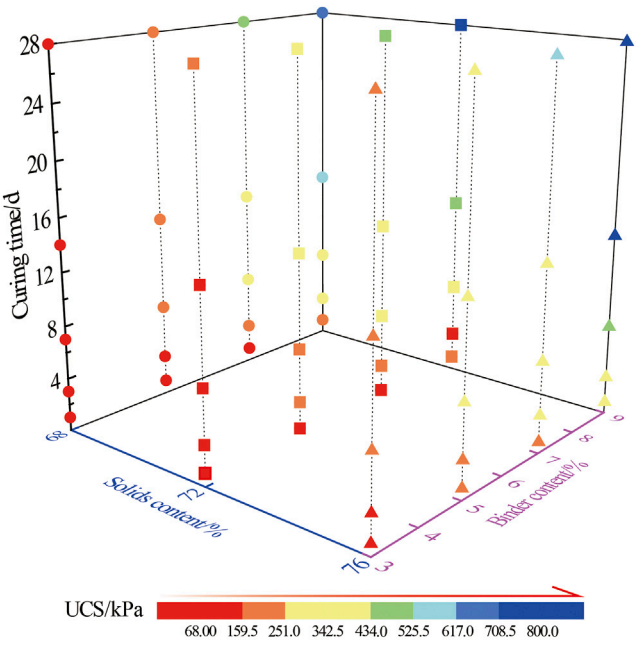

FIGURE 6 | The value of UCS corresponding to different conditions.

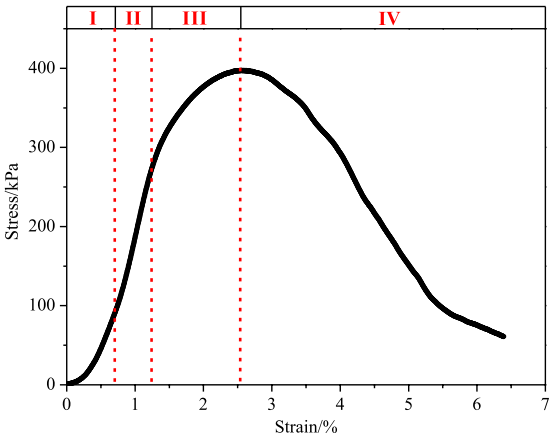

FIGURE 7 | The stress–strain curve of uniaxial compression.

sphere color shows an obvious difference when the spheres are along the *X*-axis or *Z*-axis, and the color difference of the spheres are more obvious along the direction of the *Y*-axis and the *Z*-axis.

The larger values of UCS are concentrated in the upper right area and reach the maximum UCS in this area.

In order to quantify and evaluate the variation in UCS which shows the sensitivity of UCS to the factors due to changes in curing time, binder content, and solid content, the sensitivity of UCS to the three is evaluated by defining the sensitivity coefficient *S*. Since the value ranges and spans of the curing time (1–28 days), binder content (3–9%), and solid content (68–72%) are not within the same scale, the normalized

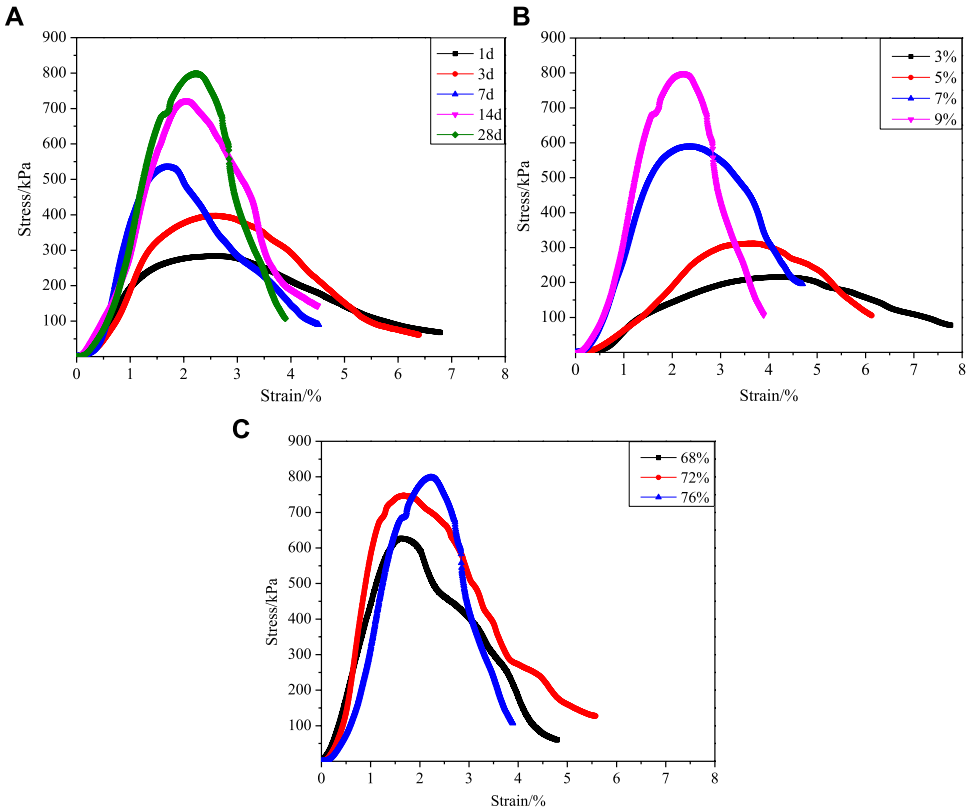

FIGURE 8 | The stress–strain curve of multi-factor. **(A)** Curves of different curing time. **(B)** Curves of different binder content. **(C)** Curves of different soild content.

parameter N_i was introduced to quantify the sensitivity of the three subsequently,

$$N_{ij} = \frac{\max\left\{\Delta m_{ij}\right\}}{\max\left\{\Delta m_{1j}, \Delta m_{2j}, \Delta m_{3j}\right\} \cdot \left(m_{ij} - m_{i1}\right)}, \tag{1}$$

$$m_{ij} = \begin{bmatrix} m_{11} & m_{12} & m_{13} & m_{14} & m_{15} \\ m_{21} & m_{22} & m_{23} & m_{24} & \\ m_{31} & m_{32} & m_{33} & & \end{bmatrix} = \begin{bmatrix} 1 & 3 & 7 & 14 & 28 \\ 3 & 5 & 7 & 9 & \\ 68 & 72 & 76 & & \end{bmatrix} \begin{matrix} i = 1, & j = 1,2,3,4,5 \\ i = 2, & j = 1,2,3,4 \\ i = 3, & j = 1,2,3 \end{matrix}, \tag{2}$$

where the subscript i is the influencing factors; the values 1, 2, and 3 indicate that the factors are curing time, binder content, and solid content, respectively; and j represents the conditions of each factor. The representative condition of m_{ij} is shown in **Eq. 2**. m_{i1} is the value of the reference condition; Δm_{ij} represents the difference between the changed value and the reference value,

$$S = \frac{R - R_0}{R_0} \cdot N_{ij}, \tag{3}$$

where S represents the sensitivity of factors, R is the value of UCS after the change, and R_0 is UCS of the reference conditions.

When the sensitivity of factors (curing time, solid content, and binder content) was analyzed, the UCS values were selected as solid content 76%,binder content 9%, curing time 1 day; the binder content 9%, curing time 28 days, solid content 68%; and solid content 76%, curing time 28 days, binder content 3% for reference conditions. Among them, the relative variation $\Delta R/R_0$ can better represent the change in UCS due to the variable value of different factors, and S is used to represent the influence of Δm to quantify the difference of UCS caused by the variation of different variable value.

As shown in **Table 4**, the relative variation $\Delta R/R_0$ shows different degrees of growth as the variable value increases under different factors. The sensitivity analysis based on the value of the sensitivity parameter shows that the value of S is small and it increases from 0.009 to 0.012 when the solid content increases to 72 and 76%, which indicates that the increase in the solid content causes a small variation in UCS, that is, UCS is weakly sensitive to solid content.

The maximum S appears when the curing time is 3 days, which UCS has the most significant variation in the curing time indicating the strongest sensitivity. The value of S is big, but it gradually decreases with the increase in curing time, indicating that the early strength is more sensitive to the curing time. S gradually increases with binder content, indicating that the sensitivity of UCS gradually increases as the cement binder increases.

Stress Evolution

The stress–strain curve can be divided into four stages according to the characteristics of the curve from **Figure 7**. Pore compaction stage (Stage Ⅰ): the curve is of "superior fovea" shape; CPB is a

heterogeneous material, in which there are more uneven "sponge" structures with pores; under the action of a small load, the "spongy" structure with pores is easy to be compressed; and the pores are tightly closed under the action of the load, which makes the CPB produce greater deformation. Elastic deformation stage (Stage II): the curve is linear in this stage, and the pores in the CPB are further compacted as the stress continues to increase. Plastic deformation stage (Stage III): In this stage, the curve is of "inferior fovea" shape, the slope of the curve gradually slows down, and the stress reaches the peak. Meanwhile, new micro-cracks sprout in the CPB, and the continuous increase in stress leads to the expansion of old cracks and the development of new cracks. Damage and failure stage (Stage IV): the curve shows obvious "softening" characteristics. The internal structure of the specimen is constantly destroyed, and the existing cracks continue to expand, gradually intersect, and merge, causing the isolated cracks to gradually penetrate, forming a macroscopic failure zone, and leading to stress drop.

The stress–strain curve of the curing time is 1, 3, 7, 14, and 28 days, for which the corresponding solid content is 76% and the binder content is 9%, which are selected to analyze the effect of curing age on the stress–strain curve in **Figure 8**. The curing time is taken as a variable. From the stress–strain curves, it can be seen that the stress–strain curves have obvious differences under different curing times, which are mainly reflected in the following three aspects: 1) The strain corresponding to UCS decreases with curing time. The strain value decreased from 2.715 to 2.225% when the curing time increases from 1 to 7 days, indicating that the deformation ability of the CPB against external loads is enhanced. When the curing age is 1 and 3 days, the phenomenon of compression swelling can be observed during the test, and it is extremely significant when the curing age is 1 day. The phenomenon can also be derived from the trend of the stress–strain curve. It can be seen that the curve appears smooth when the curing time is 1 and 3 days, and the increase in stress is small with strain. 2) The peak stress characteristics of the stress–strain curve become more obvious. With the increase in the curing time, the stress value corresponding to the later curing period increases and also the growth rate increases accordingly under the same strain condition. In the curve at the early curing period, the strain in a certain range corresponding to the peak stress is basically the same as the peak stress. When the curing time increases to 7 days, this range is significantly reduced, and the peak stress can be clearly observed. It is mainly due to an increase in the degree of binder hydration and the precipitation of a larger amount of hydration products, as well as suction increase within the CTB specimen with curing time (Xu et al., 2019). 3) The post-peak characteristics show obvious differences with the change in curing time. The stress drop caused by the internal damage of the sample increases, which can be intuitively observed from the curve shape; the smooth shape in the early curing period turns into the steep peak shape in the later curing period. Therefore, the steeper change in the post-peak response of CPB with the curing time indicates the development of CPB brittleness (Libos and Cui, 2020).

It can be seen from **Figure 8B** that with the increase in the binder content, the stress–strain curve shows obvious differences. The strain corresponding to the peak stress decreases from 4.31 to 2.225% when the binder content increases from 3 to 5% and is similar to the effect of curing time on the stress evolution, that is, the change in the binder content can enhance the peak stress characteristics and also increase the stress drop. The hydration products increase with binder content. The hydration product combines individual particles to form a skeleton structure, and the strength is derived from the cohesion and friction between the particles (Jiang et al., 2017).

From the sensitivity analysis in *Sensitivity Analysis of Multi-Factor on UCS*, it can be seen that the sensitivity of UCS to solid content is the weakest. This conclusion can be confirmed by the curves in **Figure 8C**. The curves of different solid content all show the obvious peak stress characteristics, and the difference caused by the variation of solid content is small.

CONCLUSION

In this article, a series of experiments and theoretical analysis were carried out to explore the law of the strength difference of the CPB under multi-factor coupling, quantify the sensitivity of the strength to multi-factor, and clarify the variation of stress evolution. The main conclusions are as follows:

(1) Compared with the early strength, the increase in the binder content has a greater impact on the later strength of CPB. Under the same binder content, as the increased solid content enhances the particle density inside the CPB, the UCS also increases.
(2) The sensitivity parameter was constructed considering the effect of multi-factor. The maximum values of the sensitivity parameters given by the curing time, solid content, and binder content are 0.202, 0.01, and 0.1, respectively, showing that the sensitivity of UCS to multi-factor is curing time > binder content > solid content.
(3) The curing time and binder content can effectively change the stress–strain evolution referred to three aspects: reducing the strain corresponding to the peak stress, enhancing the peak stress characteristics, and increasing the stress drop.

DATA AVAILABILITY STATEMENT

The raw data supporting the conclusions of this article will be made available by the authors, without undue reservation.

AUTHOR CONTRIBUTIONS

CH completed the writing and revision of the manuscript; LY completed the experiment, data processing and graphics drawing; and LL and BY assisted in completing the experiment.

FUNDING

This work was funded by the National Natural Science Foundation of China (Grant No.51904055), the Fundamental Research Funds for the Central Universities of China (Grant No. N2001010) and the fellowship of China Postdoctoral Science Foundation (2021MD703874). These supports are gratefully acknowledged.

REFERENCES

Cao, S., Song, W., and Yilmaz, E. (2018). Influence of Structural Factors on Uniaxial Compressive Strength of Cemented Tailings Backfill. *Construction Building Mater.* 174, 190–201. doi:10.1016/j.conbuildmat.2018.04.126

Cao, S., Xue, G., Yilmaz, E., and Yin, Z. (2021). Assessment of Rheological and Sedimentation Characteristics of Fresh Cemented Tailings Backfill Slurry. *Int. J. Mining, Reclamation Environ.* 35 (5), 319–335. doi:10.1080/17480930.2020.1826092

Chen, S., Wu, A., Wang, Y., and Wang, W. (2021). Coupled Effects of Curing Stress and Curing Temperature on Mechanical and Physical Properties of Cemented Paste Backfill. *Construction Building Mater.* 273, 121746. doi:10.1016/j.conbuildmat.2020.121746

Cui, L., and Fall, M. (2016). Mechanical and thermal Properties of Cemented Tailings Materials at Early Ages: Influence of Initial Temperature, Curing Stress and Drainage Conditions. *Construction Building Mater.* 125, 553–563. doi:10.1016/j.conbuildmat.2016.08.080

Deng, D. Q., Liu, L., Yao, Z. L., Song, K. I.-I. L., and Lao, D. Z. (2017). A Practice of Ultra-fine Tailings Disposal as Filling Material in a Gold Mine. *J. Environ. Manage.* 196, 100–109. doi:10.1016/j.jenvman.2017.02.056

Deng, H., Liu, Y., Zhang, W., Yu, S., and Tian, G. (2021). Study on the Strength Evolution Characteristics of Cemented Tailings Backfill from the Perspective of Porosity. *Minerals* 11 (1), 82. doi:10.3390/min11010082

Ding, K., Ma, F., Guo, J., Zhao, H., Lu, R., and Liu, F. (2018). Investigation of the Mechanism of Roof Caving in the Jinchuan Nickel Mine, China. *Rock Mech. Rock Eng.* 51 (4), 1215–1226. doi:10.1007/s00603-017-1374-0

Edraki, M., Baumgartl, T., Manlapig, E., Bradshaw, D., Franks, D. M., and Moran, C. J. (2014). Designing Mine Tailings for Better Environmental, Social and Economic Outcomes: a Review of Alternative Approaches. *J. Clean. Prod.* 84, 411–420. doi:10.1016/j.jclepro.2014.04.079

Ercikdi, B., Yılmaz, T., and Külekci, G. (2014). Strength and Ultrasonic Properties of Cemented Paste Backfill. *Ultrasonics* 54 (1), 195–204. doi:10.1016/j.ultras.2013.04.013

Ghirian, A., and Fall, M. (2014). Coupled Thermo-Hydro-Mechanical-Chemical Behaviour of Cemented Paste Backfill in Column Experiments. *Eng. Geology.* 170, 11–23. doi:10.1016/j.enggeo.2013.12.004

Ghirian, A., and Fall, M. (2016). Strength Evolution and Deformation Behaviour of Cemented Paste Backfill at Early Ages: Effect of Curing Stress, Filling Strategy and Drainage. *Int. J. Mining Sci. Tech.* 26 (5), 809–817. doi:10.1016/j.ijmst.2016.05.039

Gorakhki, M., and Bareither, C. (2017). Sustainable Reuse of Mine Tailings and Waste Rock as Water-Balance Covers. *Minerals* 7 (7), 128. doi:10.3390/min7070128

Hou, C., Zhu, W., Yan, B., Guan, K., and Du, J. (2018). Influence of Binder Content on Temperature and Internal Strain Evolution of Early Age Cemented Tailings Backfill. *Construction Building Mater.* 189, 585–593. doi:10.1016/j.conbuildmat.2018.09.032

Hou, Y. Q., Yin, S. H., Cao, Y., and Dai, C. Q. (2020). Analysis of Damage Characteristics and Energy Dissipation of Cemented Tailings Backfill with Different Curing Ages under Uniaxial Compression. *J. Cent. South Univ. (Science Technology)* 51 (7), 1955–1965.

Hu, C., Wang, X., Bai, R., Liu, G., Feng, X., and Ding, Q. (2018). Influence of Polyepoxysuccinic Acid on Solid Phase Products in Portland Cement Pastes. *J. Wuhan Univ. Technol.-Mat. Sci. Edit.* 33 (5), 1140–1149. doi:10.1007/s11595-018-1946-1

Jiang, G., Wu, A., Wang, Y., and Lan, W. (2018). Low Cost and High Efficiency Utilization of Hemihydrate Phosphogypsum: Used as Binder to Prepare Filling Material. *Construction Building Mater.* 167, 263–270. doi:10.1016/j.conbuildmat.2018.02.022

Jiang, H., Fall, M., and Cui, L. (2017). Freezing Behaviour of Cemented Paste Backfill Material in Column Experiments. *Construction building Mater.* 147, 837–846. doi:10.1016/j.conbuildmat.2017.05.002

Kesimal, A., Yilmaz, E., Ercikdi, B., Alp, I., and Deveci, H. (2005). Effect of Properties of Tailings and Binder on the Short-And Long-Term Strength and Stability of Cemented Paste Backfill. *Mater. Lett.* 59 (28), 3703–3709. doi:10.1016/j.matlet.2005.06.042

Li, J., Yilmaz, E., and Cao, S. (2020). Influence of Solid Content, Cement/Tailings Ratio, and Curing Time on Rheology and Strength of Cemented Tailings Backfill. *Minerals* 10 (10), 922. doi:10.3390/min10100922

Libos, I. L. S., and Cui, L. (2020). Effects of Curing Time, Cement Content, and Saturation State on Mode-I Fracture Toughness of Cemented Paste Backfill. *Eng. Fracture Mech.* 235, 107174. doi:10.1016/j.engfracmech.2020.107174

Liu, H.-l., Hou, C., Li, L., Du, J.-f., and Yan, B.-x. (2021). Experimental Investigation on Flow Properties of Cemented Paste Backfill through L-Pipe and Loop-Pipe Tests. *J. Cent. South. Univ.* 28 (9), 2830–2842. doi:10.1007/s11771-021-4810-y

Liu, L., Xin, J., Qi, C., Jia, H., and Song, K.-I. (2020). Experimental Investigation of Mechanical, Hydration, Microstructure and Electrical Properties of Cemented Paste Backfill. *Construction Building Mater.* 263, 120137. doi:10.1016/j.conbuildmat.2020.120137

Ma, S., Li, W., and Shen, X. (2019). Study on the Physical and Chemical Properties of Portland Cement with THEED. *Construction Building Mater.* 213, 617–626. doi:10.1016/j.conbuildmat.2019.03.109

Mu, W., Li, L., Guo, Z., Du, Z., and Wang, S. (2019). Novel Segmented Roadside Plugging-Filling Mining Method and Overlying Rock Mechanical Mechanism Analyses. *Energies* 12 (11), 2073. doi:10.3390/en12112073

Rong, H., Zhou, M., and Hou, H. (2017). Pore Structure Evolution and its Effect on Strength Development of Sulfate-Containing Cemented Paste Backfill. *Minerals* 7 (1), 8. doi:10.3390/min7010008

Sun, W., Wang, H., and Hou, K. (2018). Control of Waste Rock-Tailings Paste Backfill for Active Mining Subsidence Areas. *J. Clean. Prod.* 171, 567–579. doi:10.1016/j.jclepro.2017.09.253

Wu, A., Wang, Y., Wang, H., Yin, S., and Miao, X. (2015). Coupled Effects of Cement Type and Water Quality on the Properties of Cemented Paste Backfill. *Int. J. Mineral Process.* 143, 65–71. doi:10.1016/j.minpro.2015.09.004

Wu, D., Zhao, R.-k., Xie, C.-w., and Liu, S. (2020). Effect of Curing Humidity on Performance of Cemented Paste Backfill. *Int. J. Miner Metall. Mater.* 27 (8), 1046–1053. doi:10.1007/s12613-020-1970-y

Xu, L., Wang, P., and Zhang, G. (2013). Influence Mechanism of Calcium Sulfate Variety on Strength of Portland Cement-Calcium Aluminate Cement Blends. *J. Chin. Ceram. Soc.* 41 (11), 1499–1506.

Xu, W., Cao, Y., and Liu, B. (2019). Strength Efficiency Evaluation of Cemented Tailings Backfill with Different Stratified Structures. *Eng. Structures* 180, 18–28. doi:10.1016/j.engstruct.2018.11.030

Xu, W., Tian, X., and Cao, P. (2018). Assessment of Hydration Process and Mechanical Properties of Cemented Paste Backfill by Electrical Resistivity Measurement. *Nondestructive Test. Eval.* 33 (2), 198–212. doi:10.1080/10589759.2017.1353983

Yilmaz, E. (2011). Advances in Reducing Large Volumes of Environmentally Harmful Mine Waste Rocks and Tailings. *Gospodarka Surowcami Mineralnymi* 27, 89–112.

Zhang, Y., Yu, P., Pan, F., and He, Y. (2018). The Synergistic Effect of AFt Enhancement and Expansion in Portland Cement-Aluminate Cement-FGD gypsum Composite Cementitious System. *Construction Building Mater.* 190, 985–994. doi:10.1016/j.conbuildmat.2018.09.139

Conflict of Interest: The authors declare that the research was conducted in the absence of any commercial or financial relationships that could be construed as a potential conflict of interest.

Publisher's Note: All claims expressed in this article are solely those of the authors and do not necessarily represent those of their affiliated organizations, or those of the publisher, the editors and the reviewers. Any product that may be evaluated in this article, or claim that may be made by its manufacturer, is not guaranteed or endorsed by the publisher.